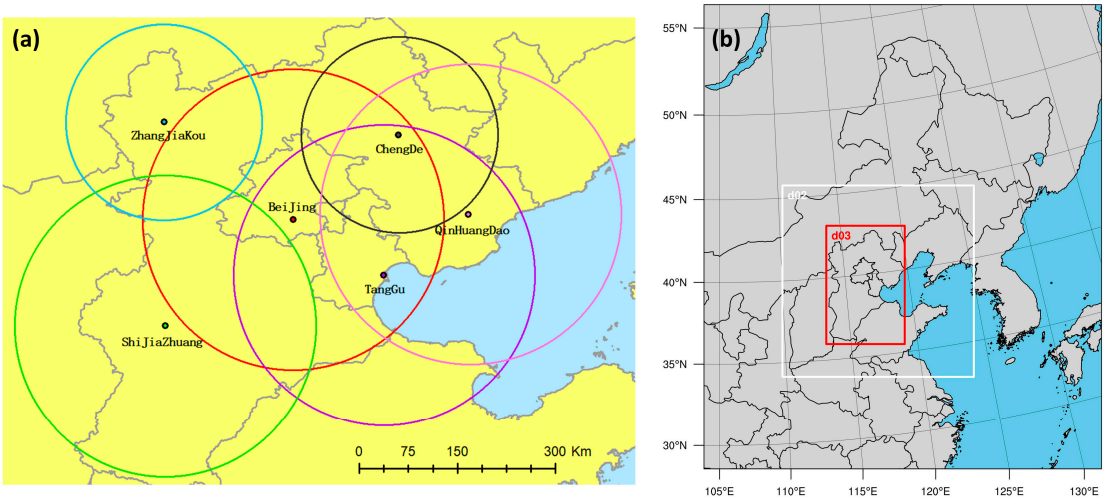

Figure S1. (a): The selected six radar stations in the Beijing-Tianjin-Hebei region. (b): WRF simulation area with three nested domains.

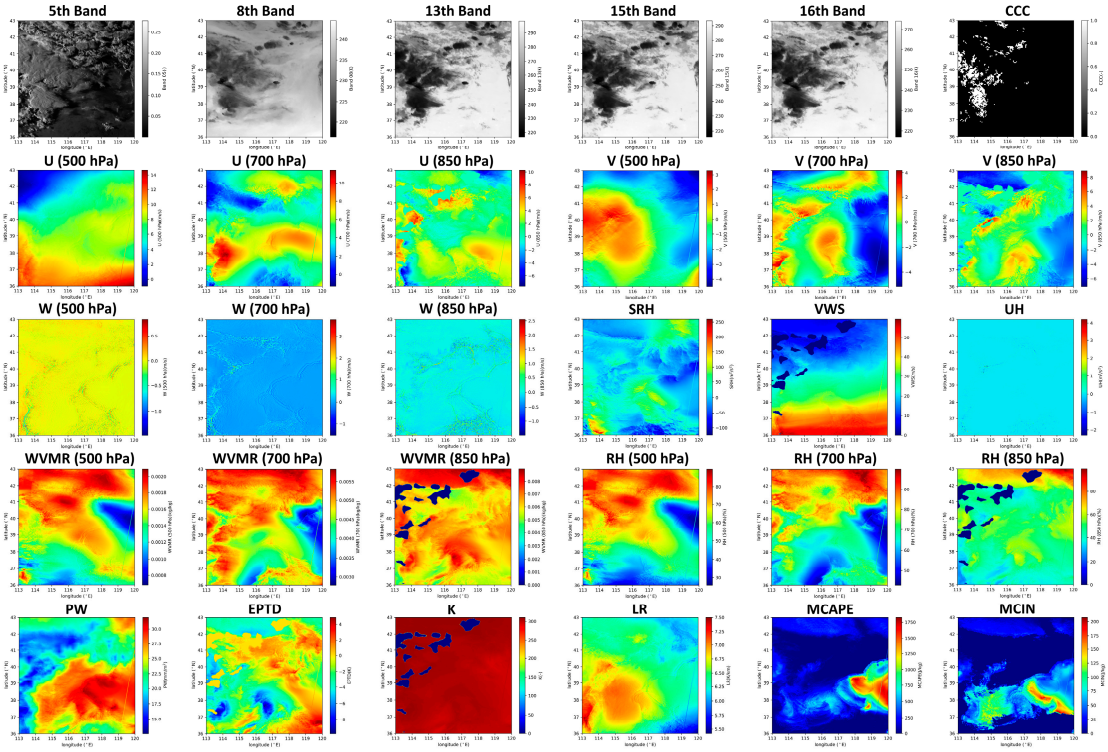

Figure S2. Visualizations of input data of the reconstruction sample at 09:30 UTC on 10 September 2016.

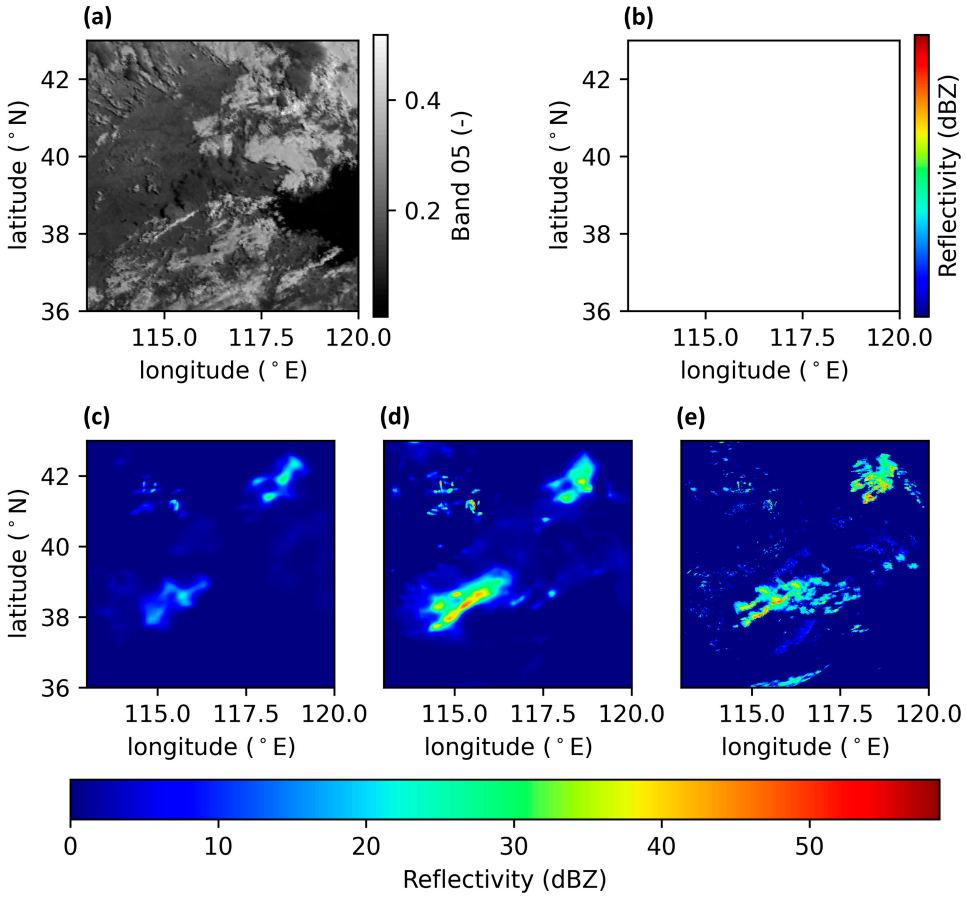

Figure S3. A case of reconstruction at 00:30 UTC on 4 September 2016 from the test set. (a) The satellite image of the 5th band. (b) The WRF-simulated reflectivity data. (c) The echo reconstruction by the UNet-MSE network. (d) The echo reconstruction by the UNet-EW network. (e) The observed radar reflectivity data.

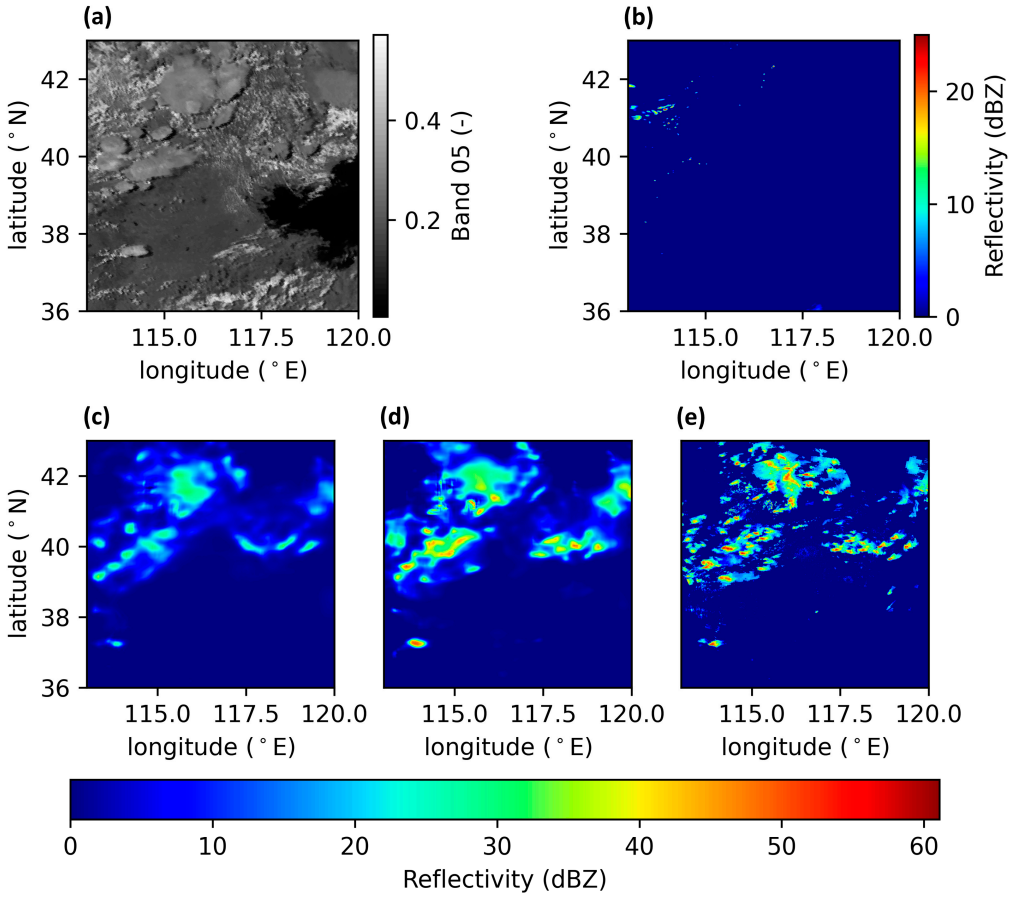

Figure S4. A case of reconstruction at 05:30 UTC on 4 September 2016 from the test set. (a) The satellite image of the 5th band. (b) The WRF-simulated reflectivity data. (c) The echo reconstruction by the UNet-MSE network. (d) The echo reconstruction by the UNet-EW network. (e) The observed radar reflectivity data.

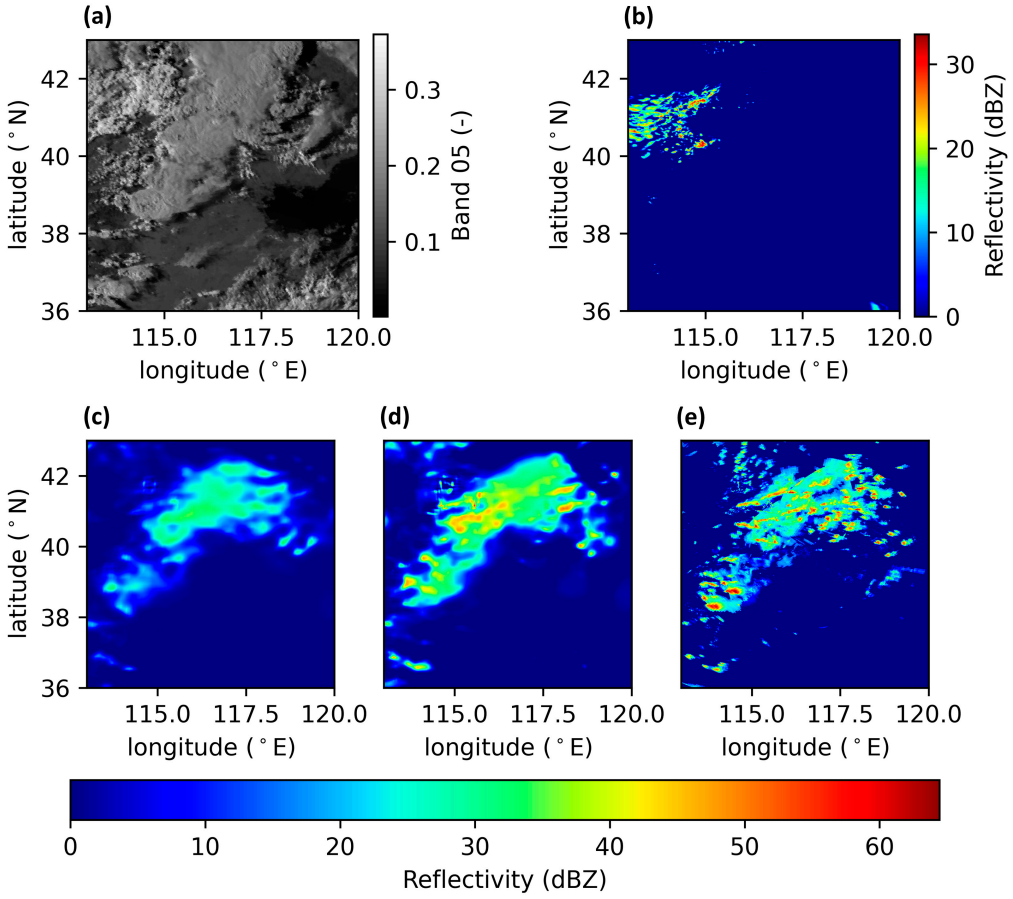

Figure S5. A case of reconstruction at 08:30 UTC on 4 September 2016 from the test set. (a) The satellite image of the 5th band. (b) The WRF-simulated reflectivity data. (c) The echo reconstruction by the UNet-MSE network. (d) The echo reconstruction by the UNet-EW network. (e) The observed radar reflectivity data.

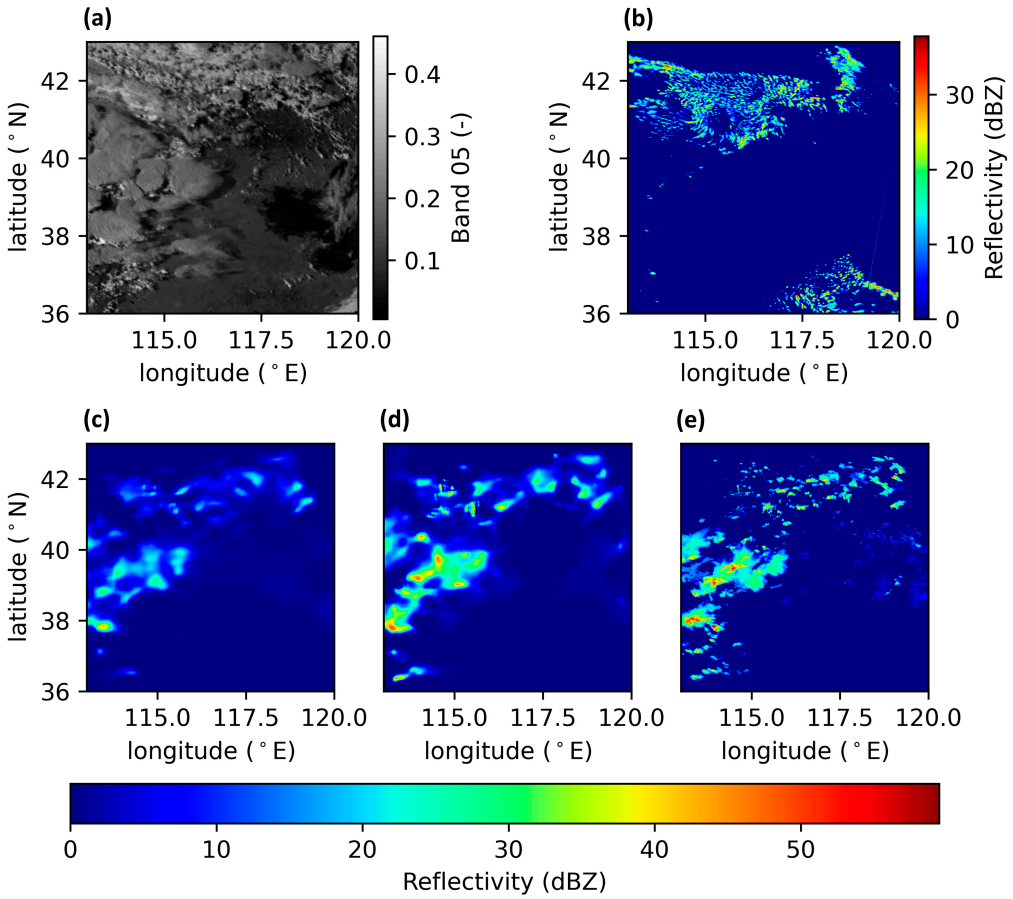

Figure S6. A case of reconstruction at 08:00 UTC on 10 September 2016 from the test set. (a) The satellite image of the 5th band. (b) The WRF-simulated reflectivity data. (c) The echo reconstruction by the UNet-MSE network. (d) The echo reconstruction by the UNet-EW network. (e) The observed radar reflectivity data.

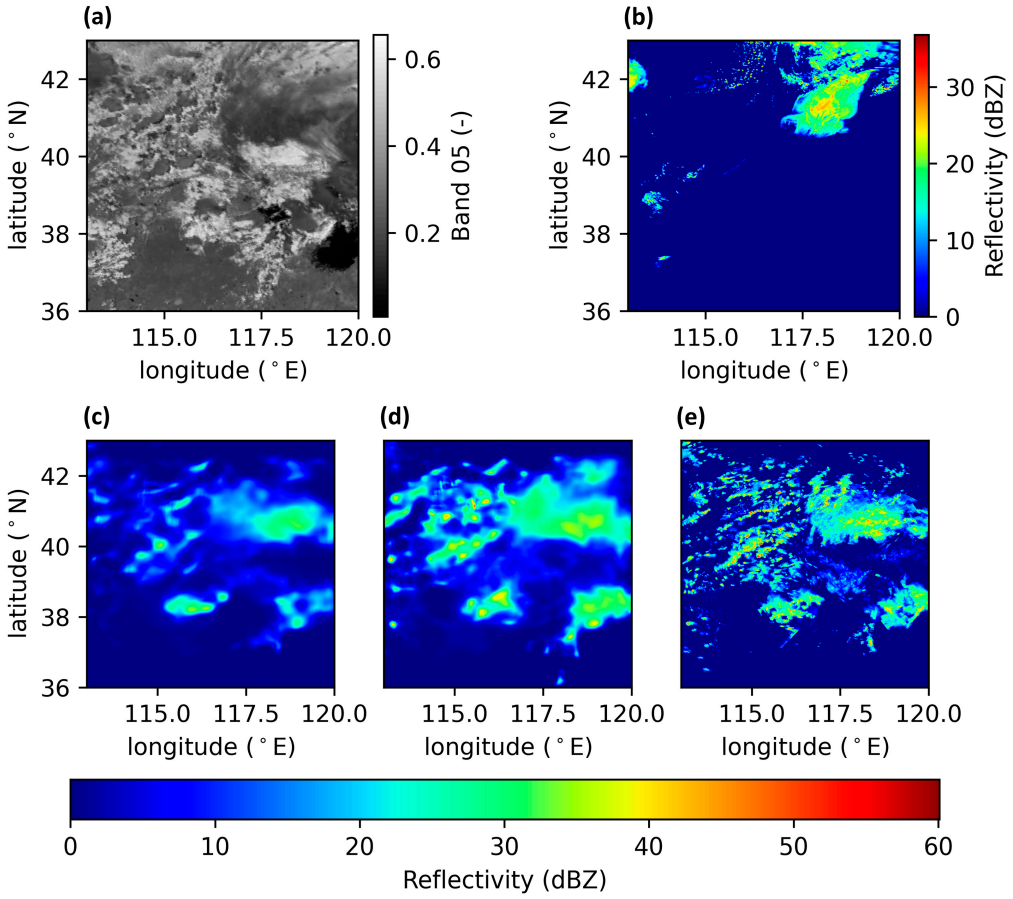

Figure S7. A case of reconstruction at 03:30 UTC on 11 September 2016 from the test set. (a) The satellite image of the 5th band. (b) The WRF-simulated reflectivity data. (c) The echo reconstruction by the UNet-MSE network. (d) The echo reconstruction by the UNet-EW network. (e) The observed radar reflectivity data.

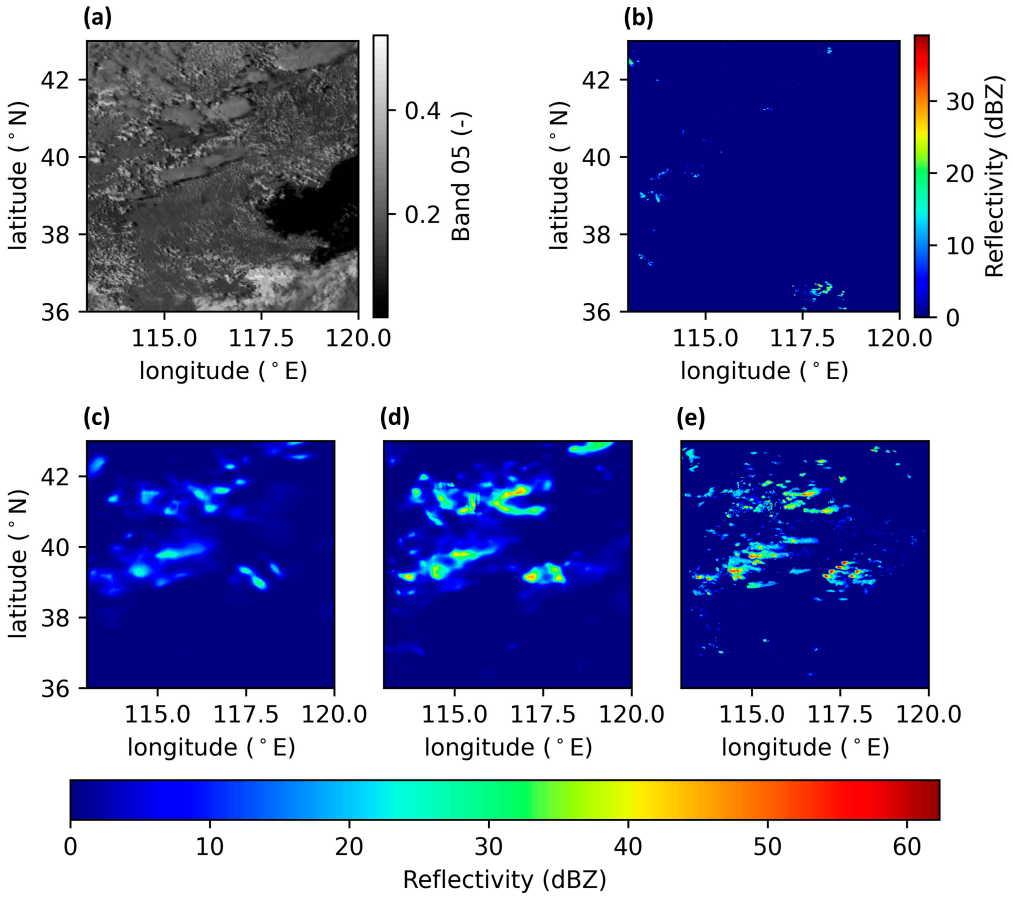

Figure S8. A case of reconstruction at 06:30 UTC on 13 September 2016 from the test set. (a) The satellite image of the 5th band. (b) The WRF-simulated reflectivity data. (c) The echo reconstruction by the UNet-MSE network. (d) The echo reconstruction by the UNet-EW network. (e) The observed radar reflectivity data.

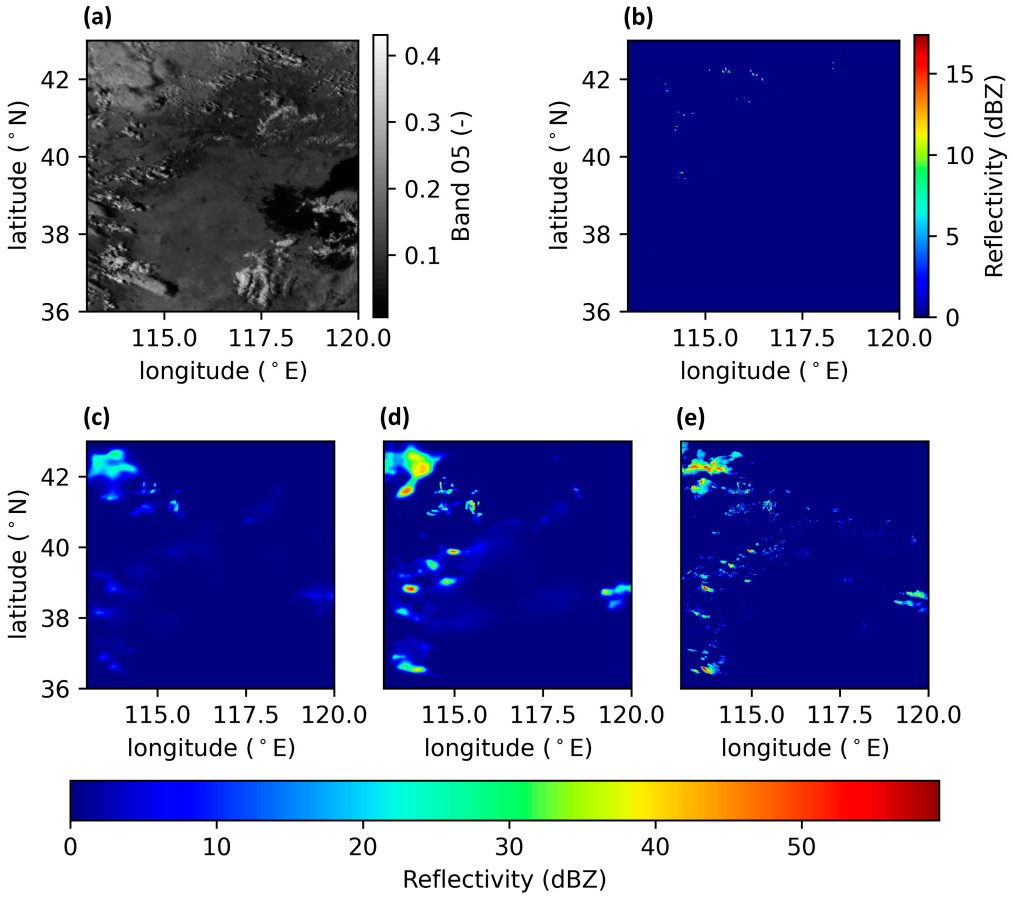

Figure S9. A case of reconstruction at 07:30 UTC on 23 September 2016 from the test set. (a) The satellite image of the 5th band. (b) The WRF-simulated reflectivity data. (c) The echo reconstruction by the UNet-MSE network. (d) The echo reconstruction by the UNet-EW network. (e) The observed radar reflectivity data.

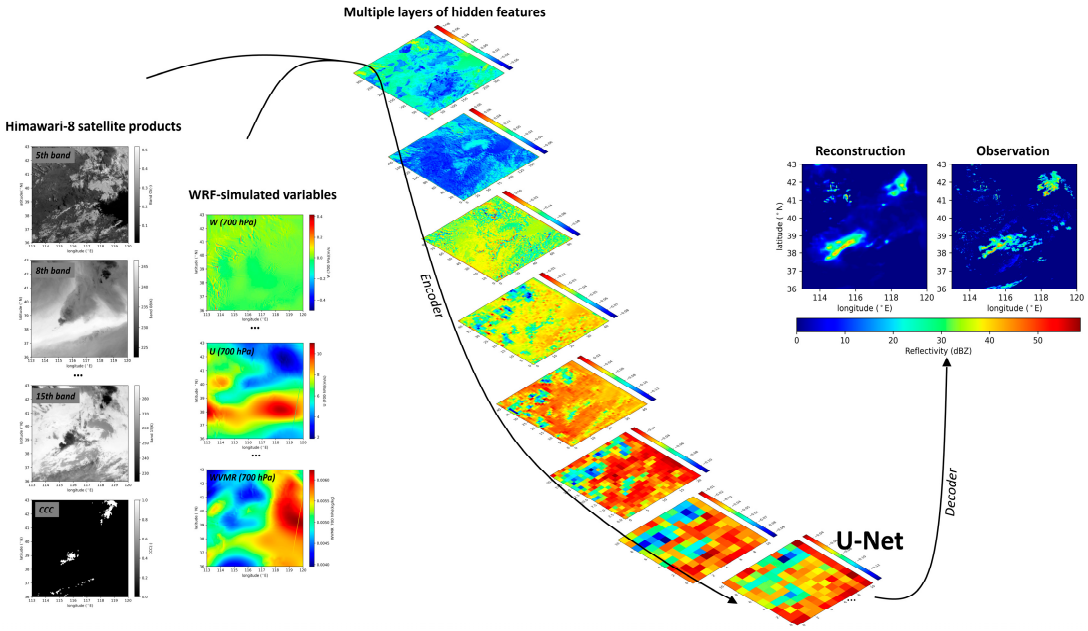

Figure S10. A multiscale representation of the radar echo data at 00:30 UTC on 4 September 2016. The UNet-EW deep network is used for the reconstruction of echo data. Only parts of the input data for this reconstruction are presented.

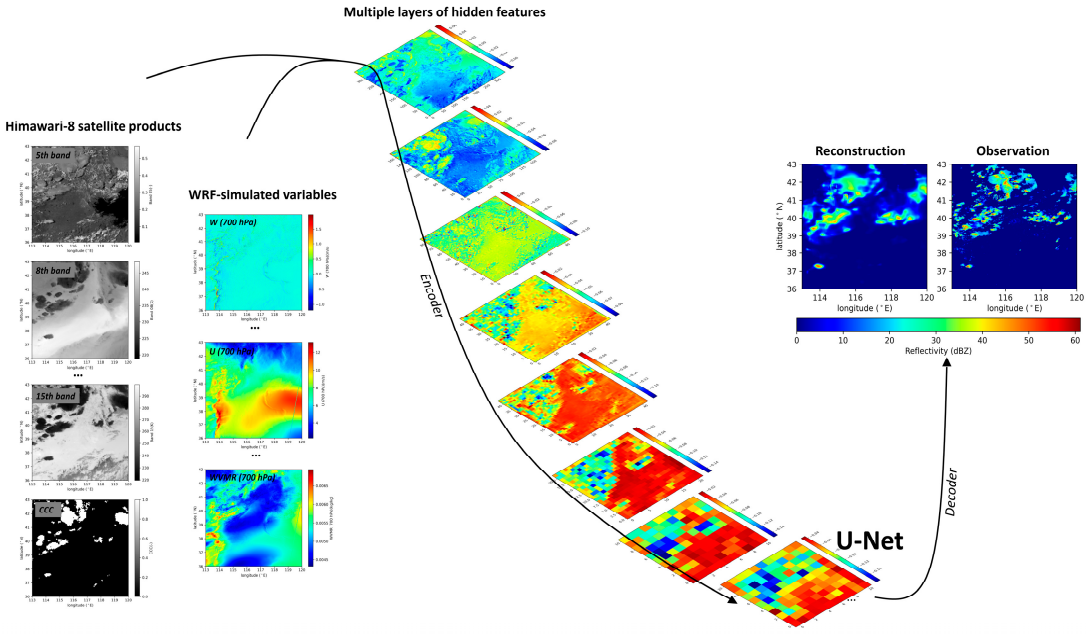

Figure S11. A multiscale representation of the radar echo data at 05:30 UTC on 4 September 2016. The UNet-EW deep network is used for the reconstruction of echo data. Only parts of the input data for this reconstruction are presented.

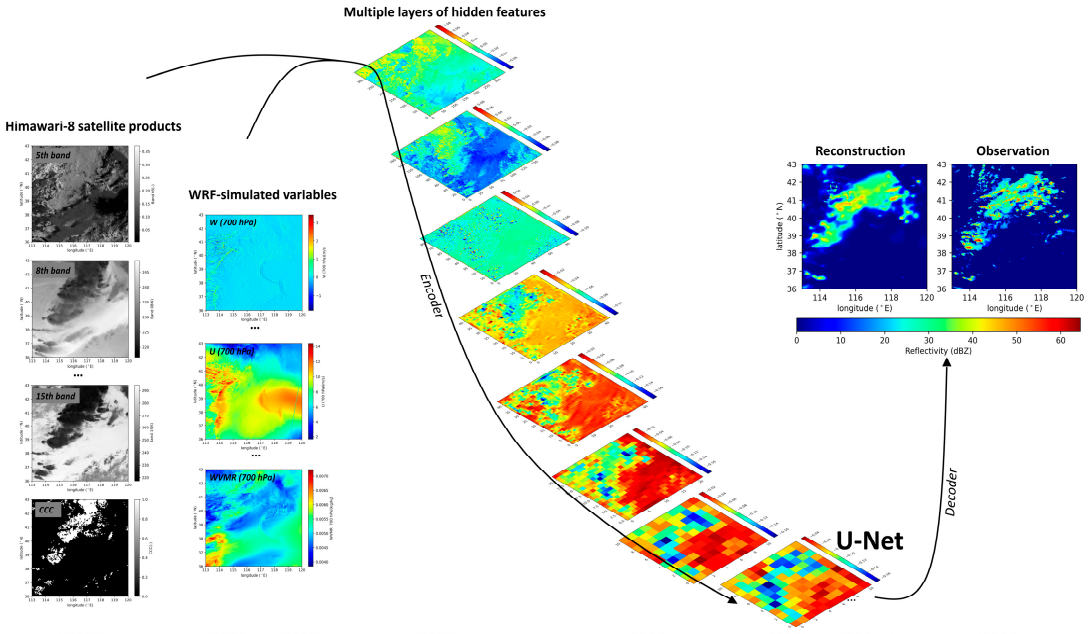

Figure S12. A multiscale representation of the radar echo data at 08:30 UTC on 4 September 2016. The UNet-EW deep network is used for the reconstruction of echo data. Only parts of the input data for this reconstruction are presented.

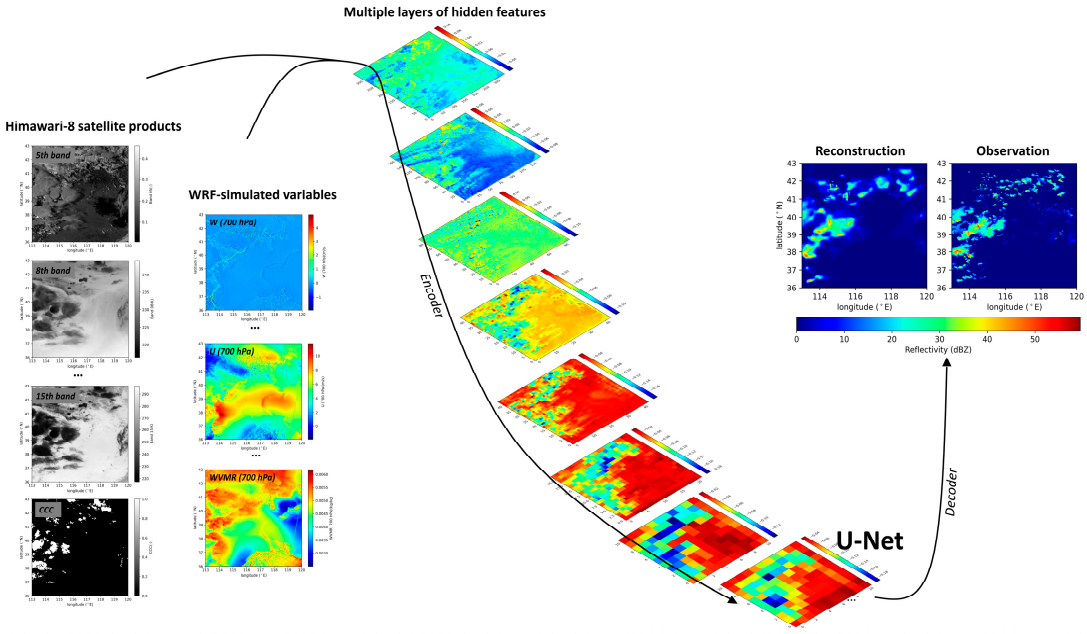

Figure S13. A multiscale representation of the radar echo data at 08:00 UTC on 10 September 2016. The UNet-EW deep network is used for the reconstruction of echo data. Only parts of the input data for this reconstruction are presented.

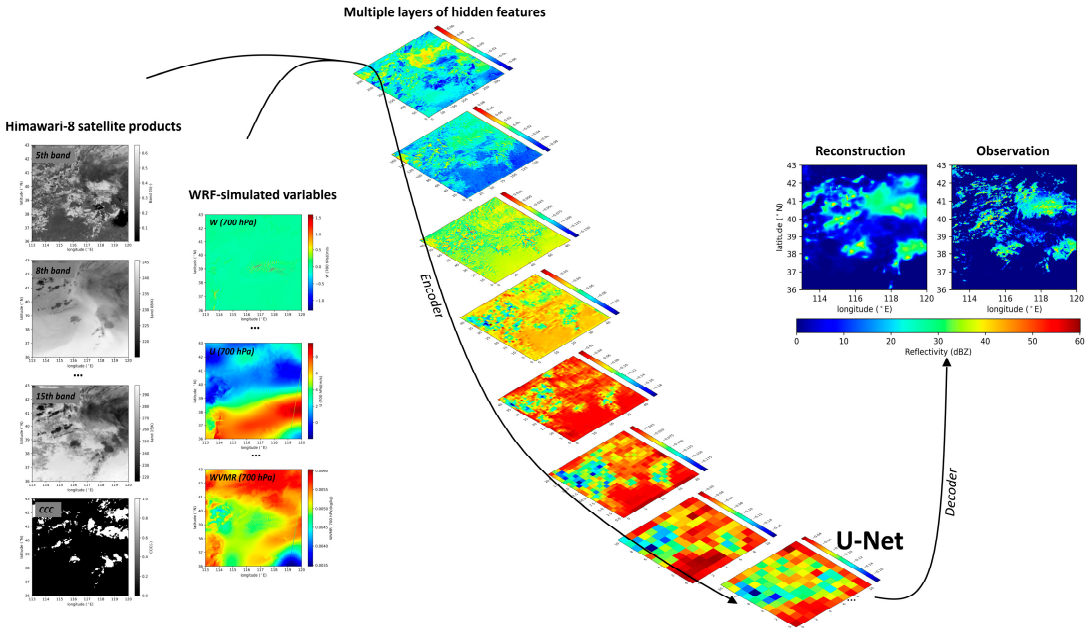

Figure S14. A multiscale representation of the radar echo data at 03:30 UTC on 11 September 2016. The UNet-EW deep network is used for the reconstruction of echo data. Only parts of the input data for this reconstruction are presented.

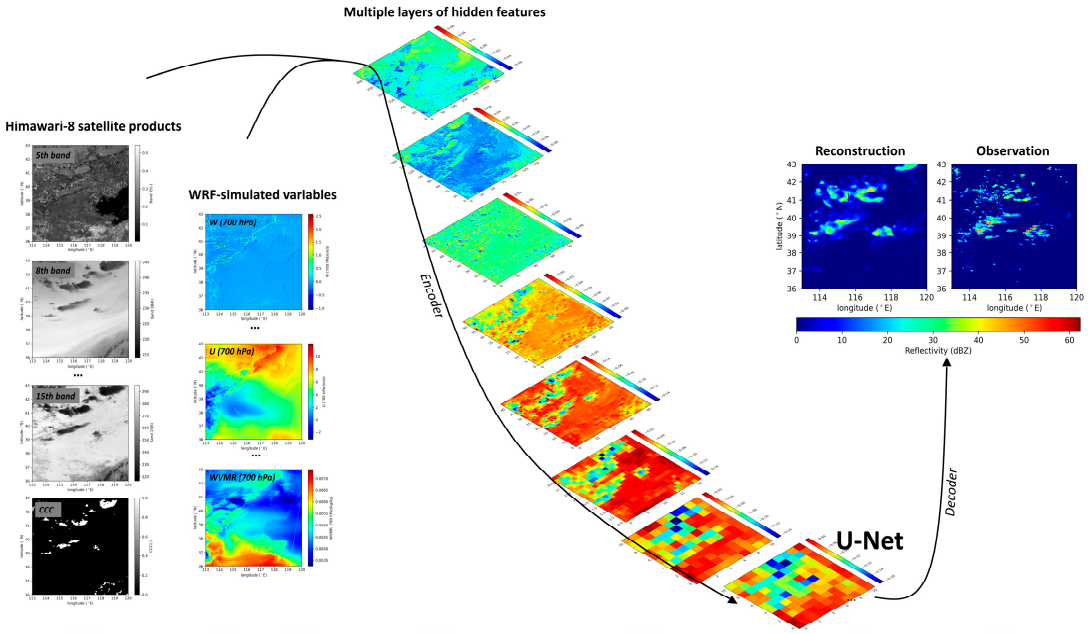

Figure S15. A multiscale representation of the radar echo data at 06:30 UTC on 13 September 2016. The UNet-EW deep network is used for the reconstruction of echo data. Only parts of the input data for this reconstruction are presented.

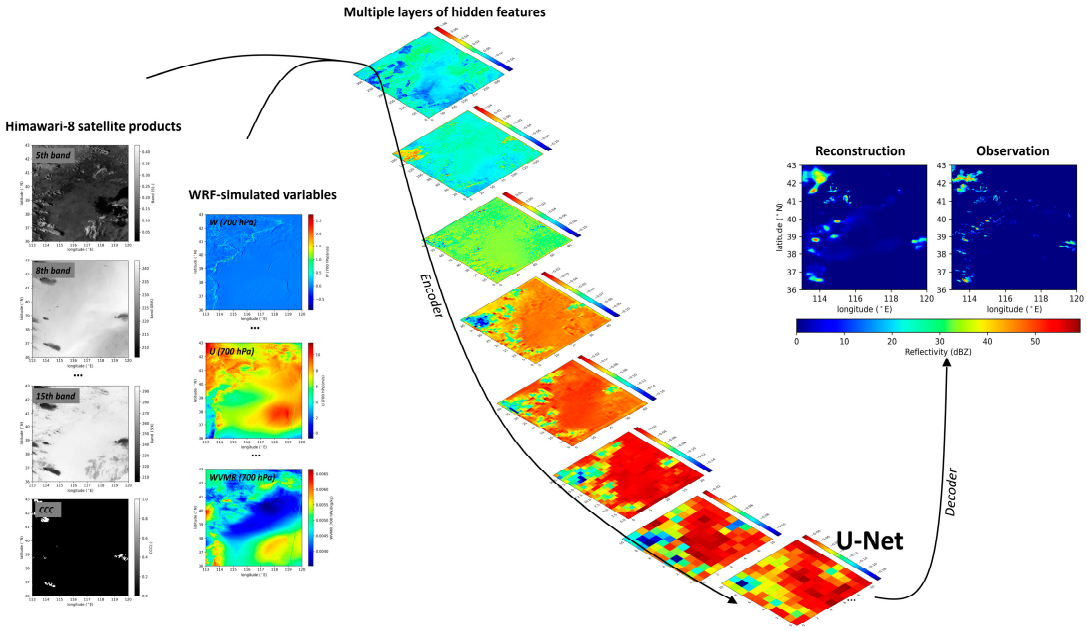

Figure S16. A multiscale representation of the radar echo data at 07:30 UTC on 23 September 2016. The UNet-EW deep network is used for the reconstruction of echo data. Only parts of the input data for this reconstruction are presented.

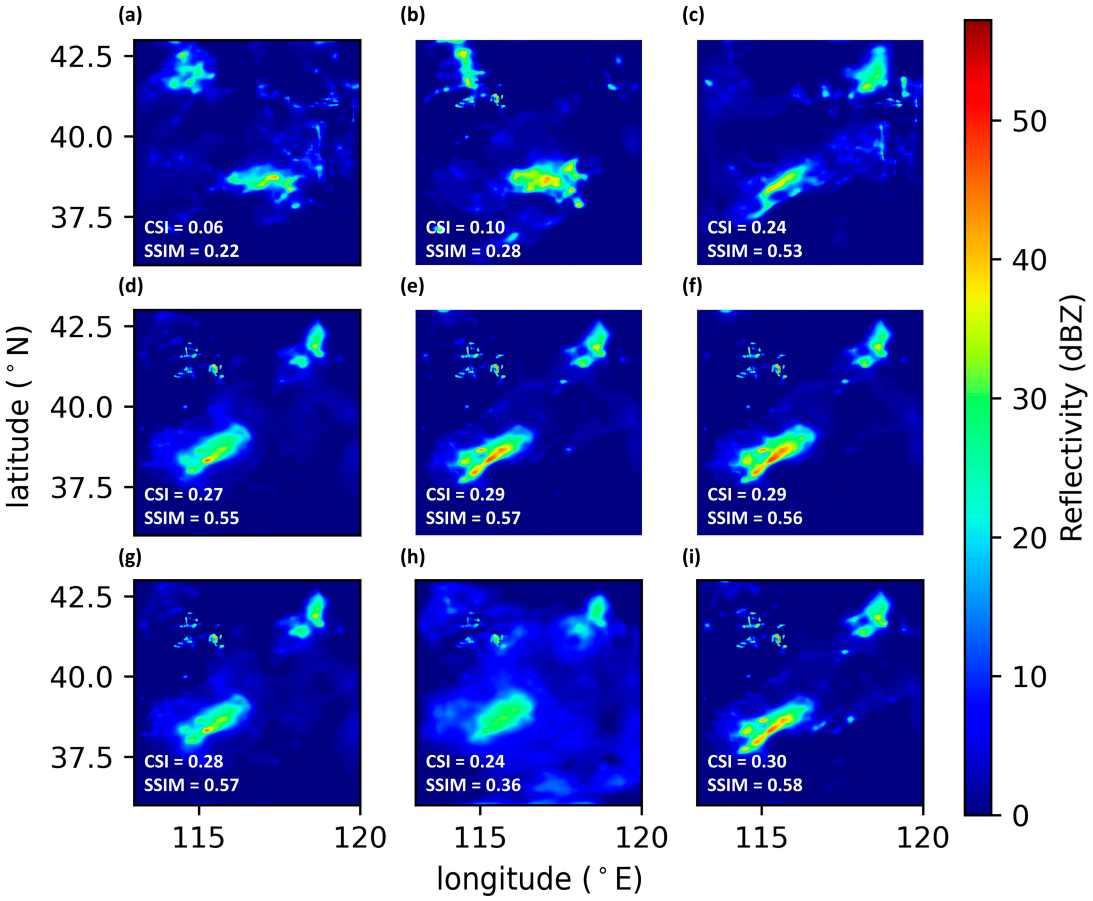

Figure S17. Reconstructions of the radar echo data at 00:30 UTC on 4 September 2016 by the UNet-EW deep network for the SA-a experiments. The perturbations are conducted by (a) flipping all the input data, (b) flipping only the satellite images, (c) flipping only the WRF simulations, (d) multiplying all the input data (except for the binary CCC data) by 0.9, (e) multiplying only the satellite images (except for the binary CCC data) by 0.9 and (f) 0.8, and (g) multiplying only the WRF simulations by 0.9 and (h) 0.8. Also shown is the (i) original reconstruction without perturbation.

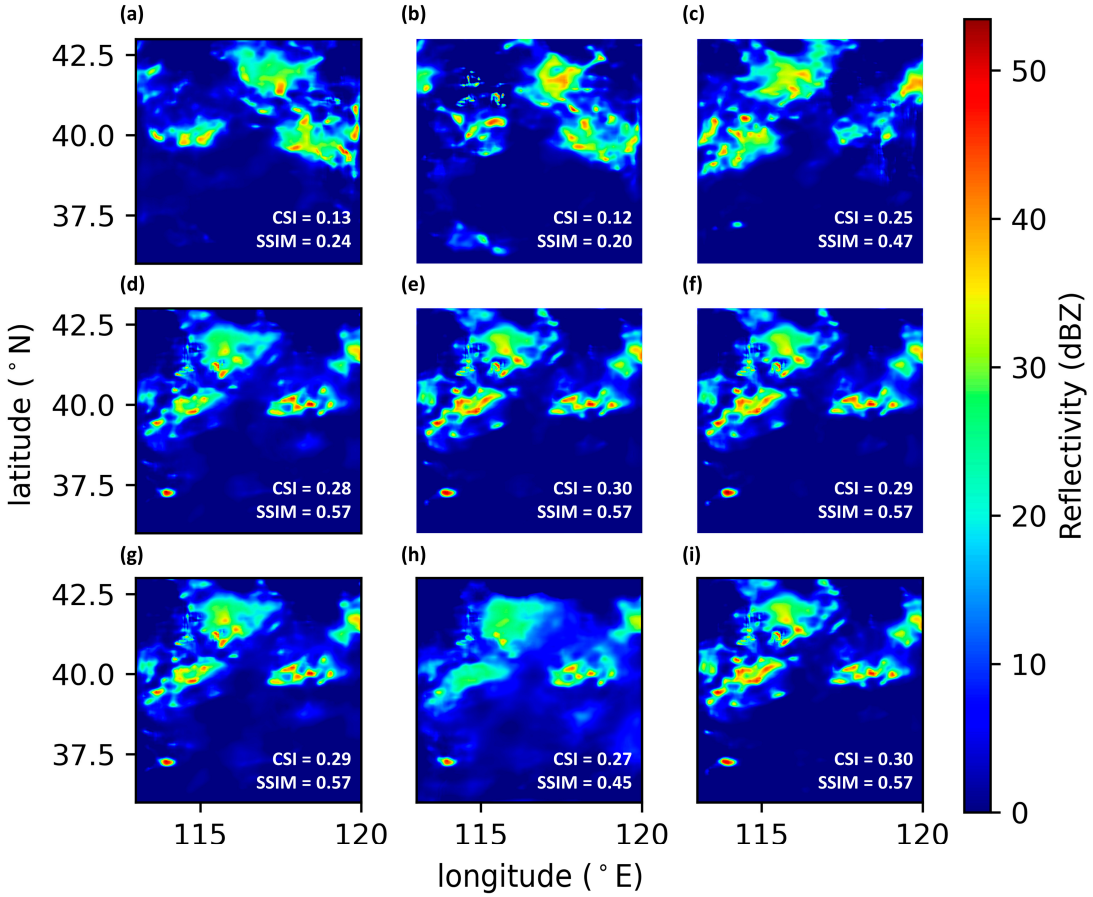

Figure S18. Reconstructions of the radar echo data at 05:30 UTC on 4 September 2016 by the UNet-EW deep network for the SA-a experiments. The perturbations are conducted by (a) flipping all the input data, (b) flipping only the satellite images, (c) flipping only the WRF simulations, (d) multiplying all the input data (except for the binary CCC data) by 0.9, (e) multiplying only the satellite images (except for the binary CCC data) by 0.9 and (f) 0.8, and (g) multiplying only the WRF simulations by 0.9 and (h) 0.8. Also shown is the (i) original reconstruction without perturbation.

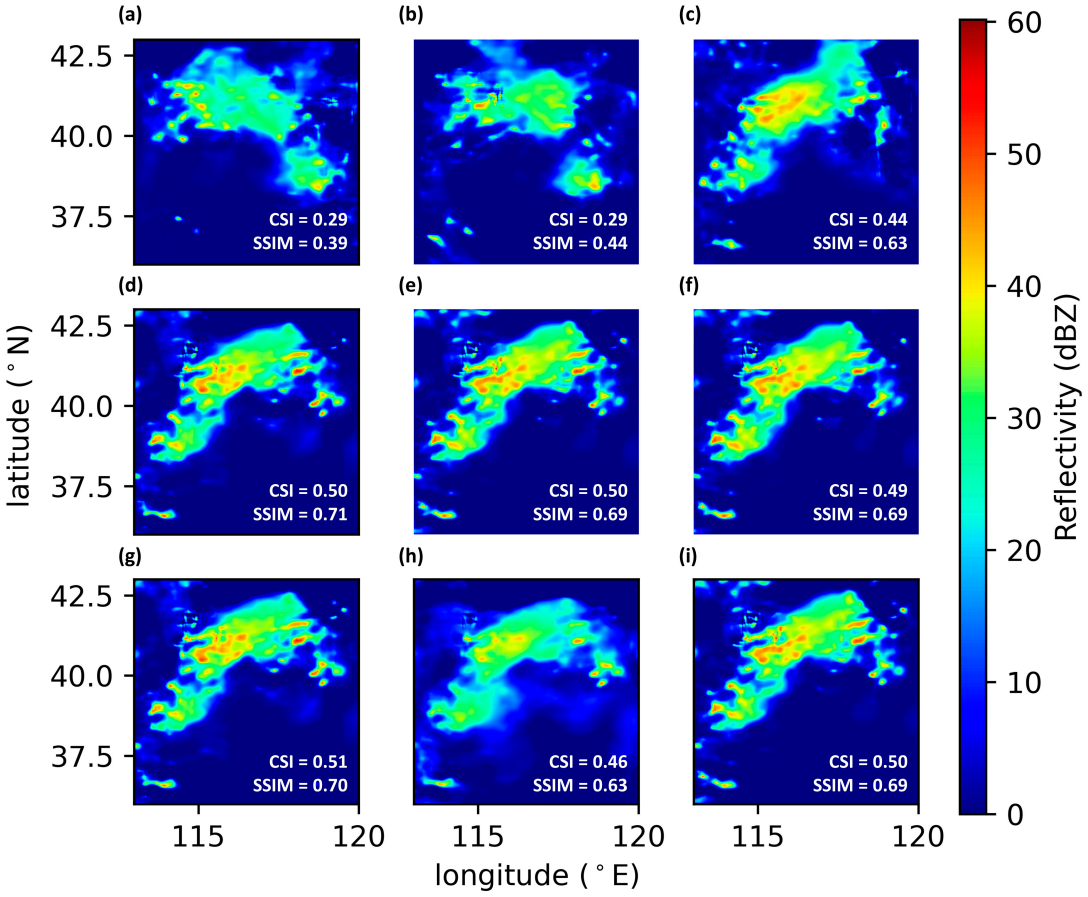

Figure S19. Reconstructions of the radar echo data at 08:30 UTC on 4 September 2016 by the UNet-EW deep network for the SA-a experiments. The perturbations are conducted by (a) flipping all the input data, (b) flipping only the satellite images, (c) flipping only the WRF simulations, (d) multiplying all the input data (except for the binary CCC data) by 0.9, (e) multiplying only the satellite images (except for the binary CCC data) by 0.9 and (f) 0.8, and (g) multiplying only the WRF simulations by 0.9 and (h) 0.8. Also shown is the (i) original reconstruction without perturbation.

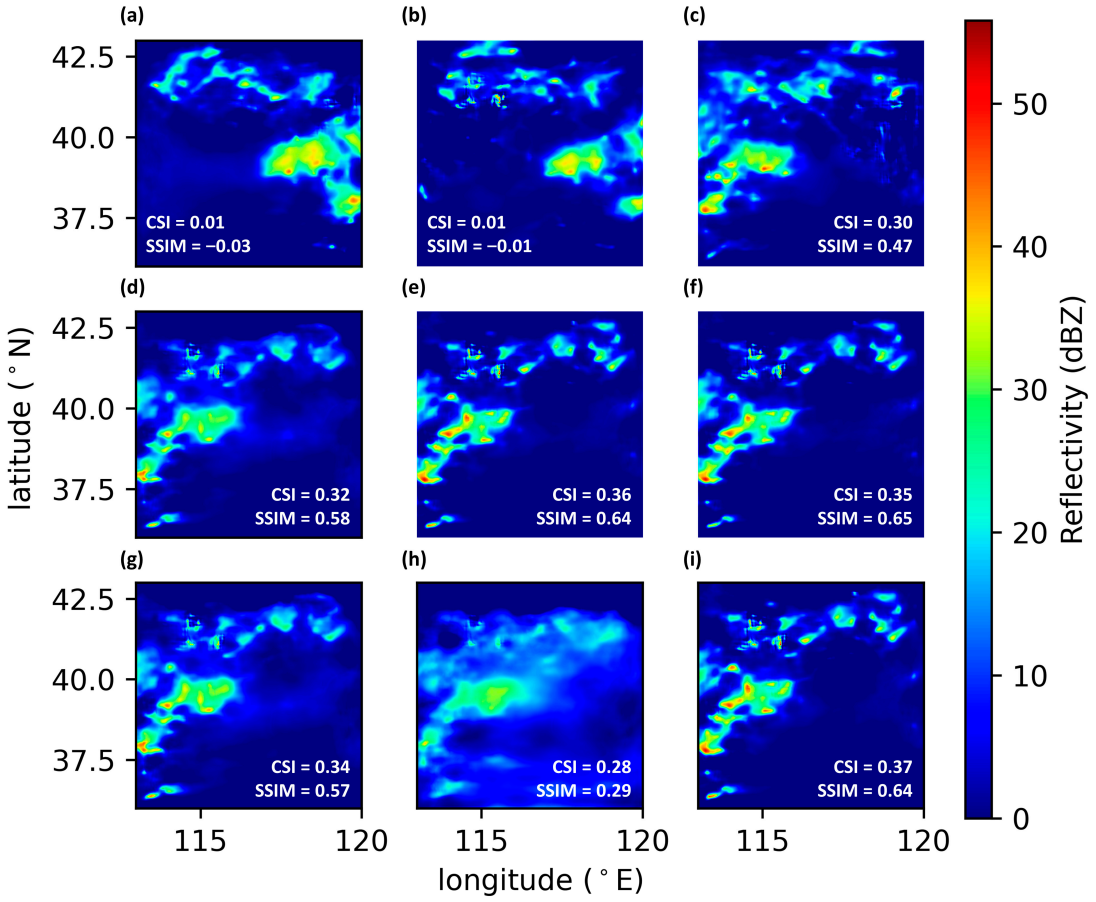

Figure S20. Reconstructions of the radar echo data at 08:00 UTC on 10 September 2016 by the UNet-EW deep network for the SA-a experiments. The perturbations are conducted by (a) flipping all the input data, (b) flipping only the satellite images, (c) flipping only the WRF simulations, (d) multiplying all the input data (except for the binary CCC data) by 0.9, (e) multiplying only the satellite images (except for the binary CCC data) by 0.9 and (f) 0.8, and (g) multiplying only the WRF simulations by 0.9 and (h) 0.8. Also shown is the (i) original reconstruction without perturbation.

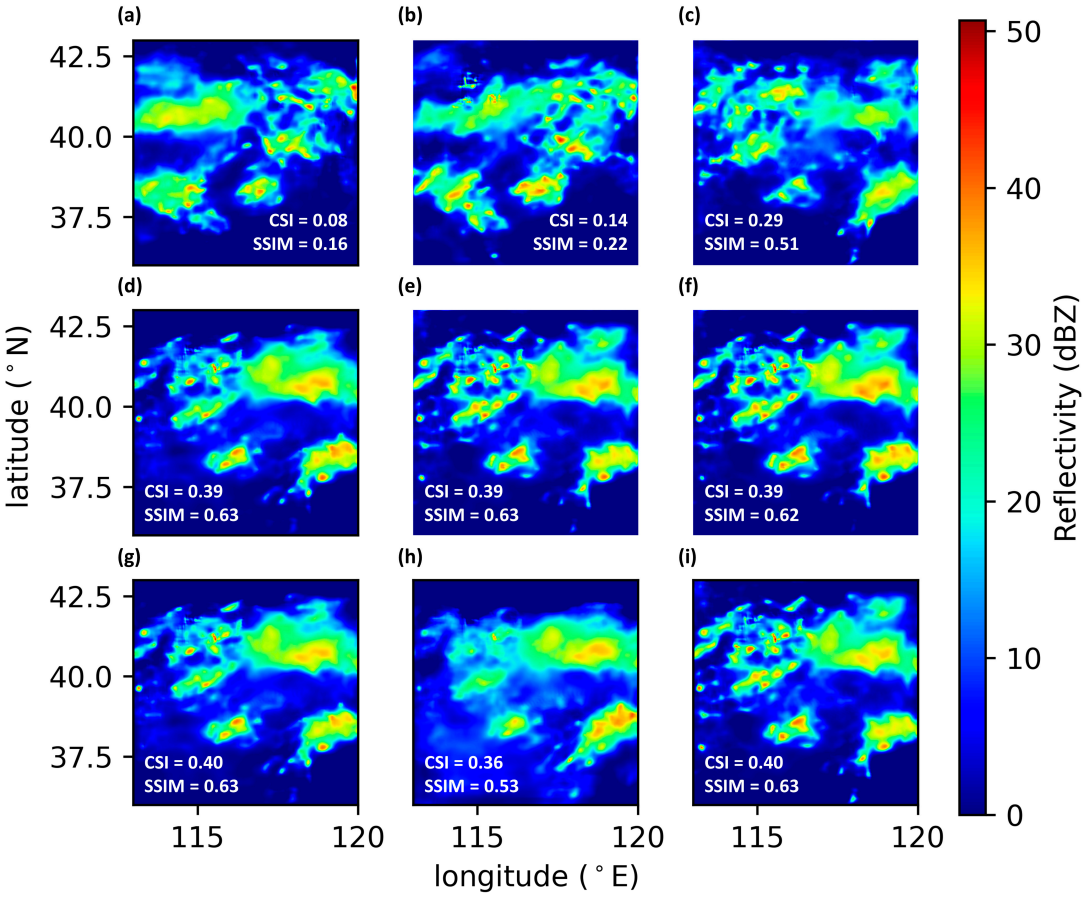

Figure S21. Reconstructions of the radar echo data at 03:30 UTC on 11 September 2016 by the UNet-EW deep network for the SA-a experiments. The perturbations are conducted by (a) flipping all the input data, (b) flipping only the satellite images, (c) flipping only the WRF simulations, (d) multiplying all the input data (except for the binary CCC data) by 0.9, (e) multiplying only the satellite images (except for the binary CCC data) by 0.9 and (f) 0.8, and (g) multiplying only the WRF simulations by 0.9 and (h) 0.8. Also shown is the (i) original reconstruction without perturbation.

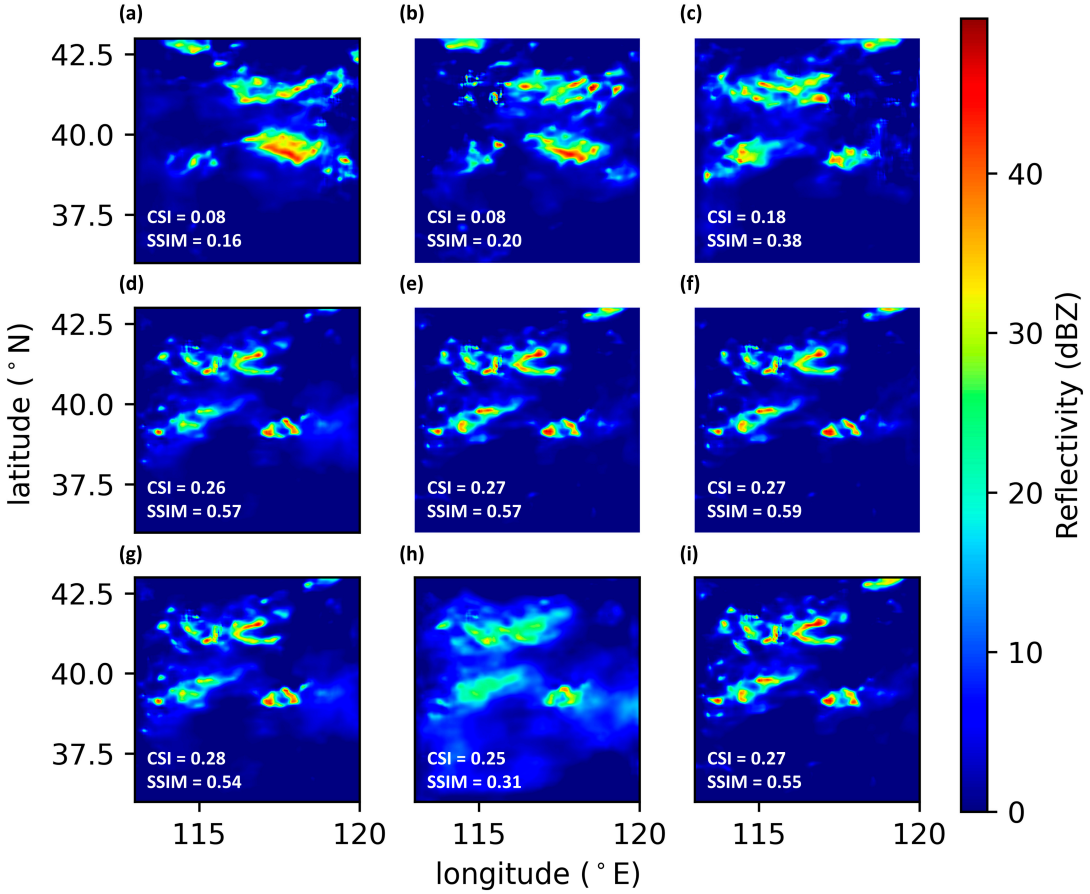

Figure S22. Reconstructions of the radar echo data at 06:30 UTC on 13 September 2016 by the UNet-EW deep network for the SA-a experiments. The perturbations are conducted by (a) flipping all the input data, (b) flipping only the satellite images, (c) flipping only the WRF simulations, (d) multiplying all the input data (except for the binary CCC data) by 0.9, (e) multiplying only the satellite images (except for the binary CCC data) by 0.9 and (f) 0.8, and (g) multiplying only the WRF simulations by 0.9 and (h) 0.8. Also shown is the (i) original reconstruction without perturbation.

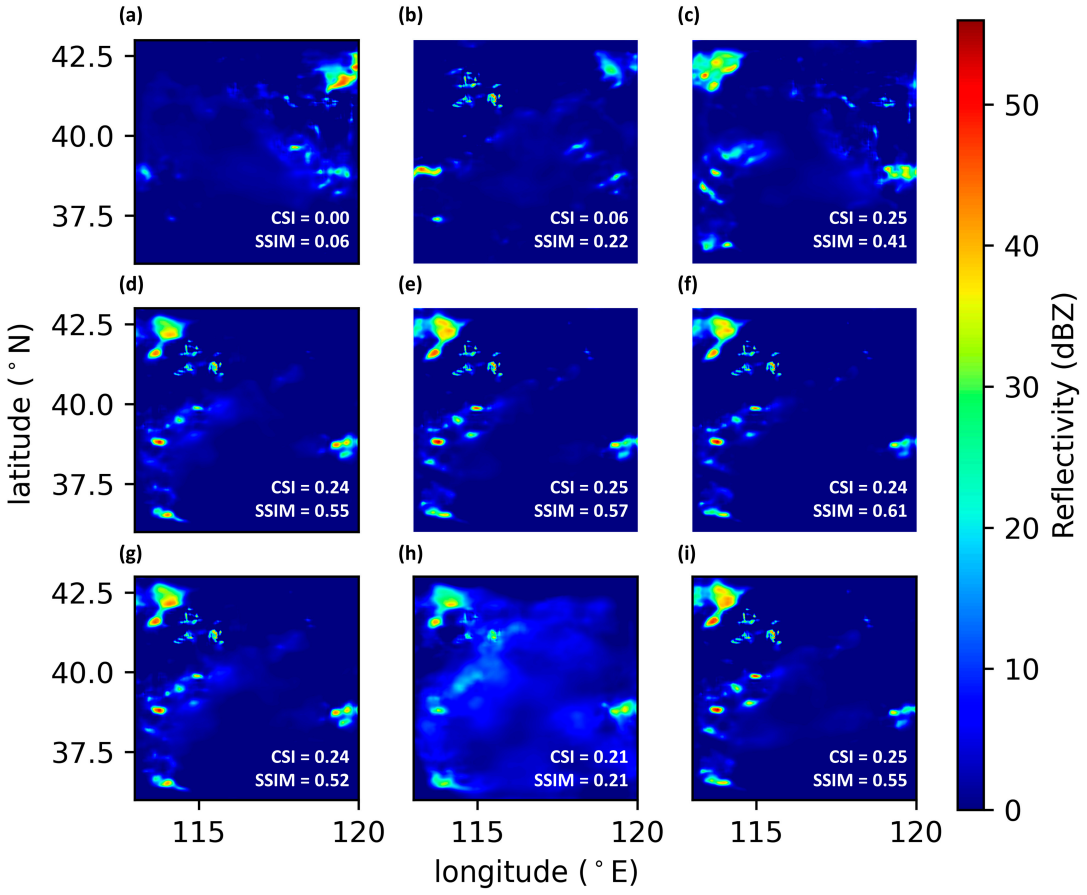

Figure S23. Reconstructions of the radar echo data at 07:30 UTC on 23 September 2016 by the UNet-EW deep network for the SA-a experiments. The perturbations are conducted by (a) flipping all the input data, (b) flipping only the satellite images, (c) flipping only the WRF simulations, (d) multiplying all the input data (except for the binary CCC data) by 0.9, (e) multiplying only the satellite images (except for the binary CCC data) by 0.9 and (f) 0.8, and (g) multiplying only the WRF simulations by 0.9 and (h) 0.8. Also shown is the (i) original reconstruction without perturbation.

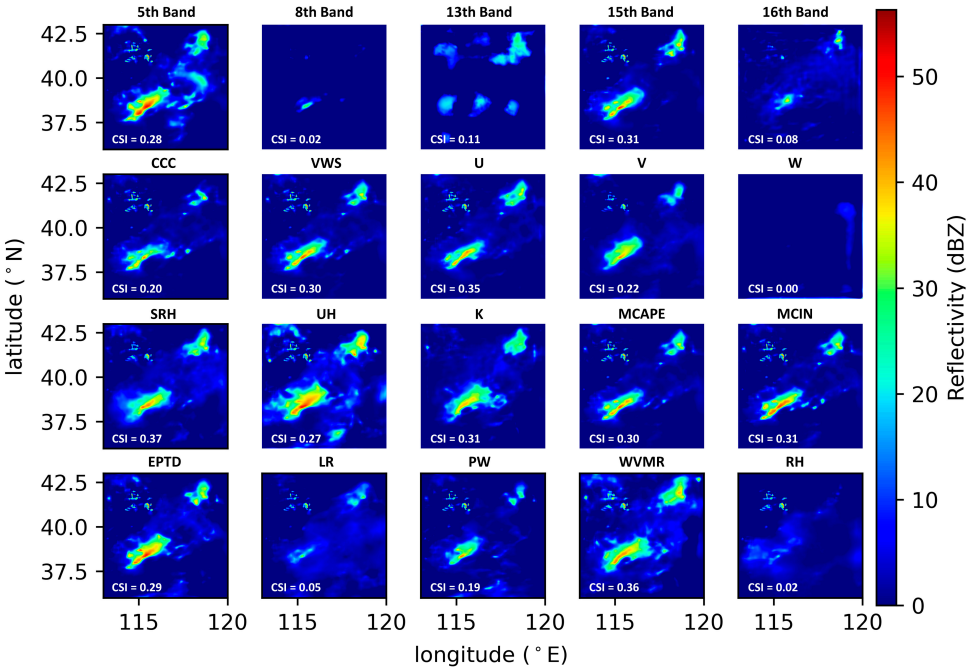

Figure S24. Reconstructions of the radar echo data at 00:30 UTC on 4 September 2016 by the UNet-EW deep network for the SA-b experiments. Each reconstruction is obtained by setting the listed physical quantity to zero while keeping other quantities unchanged.

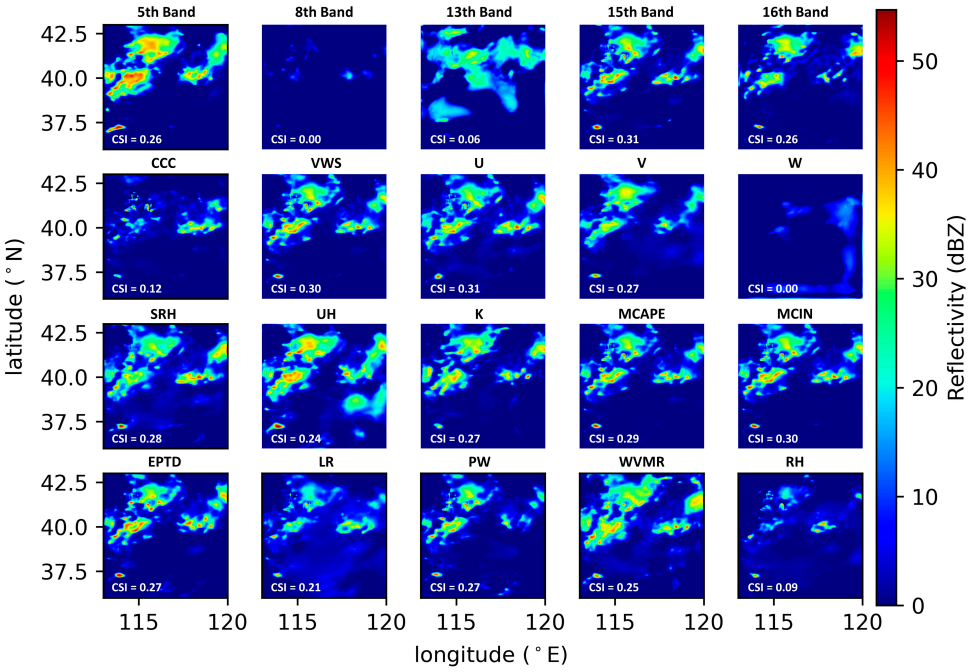

Figure S25. Reconstructions of the radar echo data at 05:30 UTC on 4 September 2016 by the UNet-EW deep network for the SA-b experiments. Each reconstruction is obtained by setting the listed physical quantity to zero while keeping other quantities unchanged.

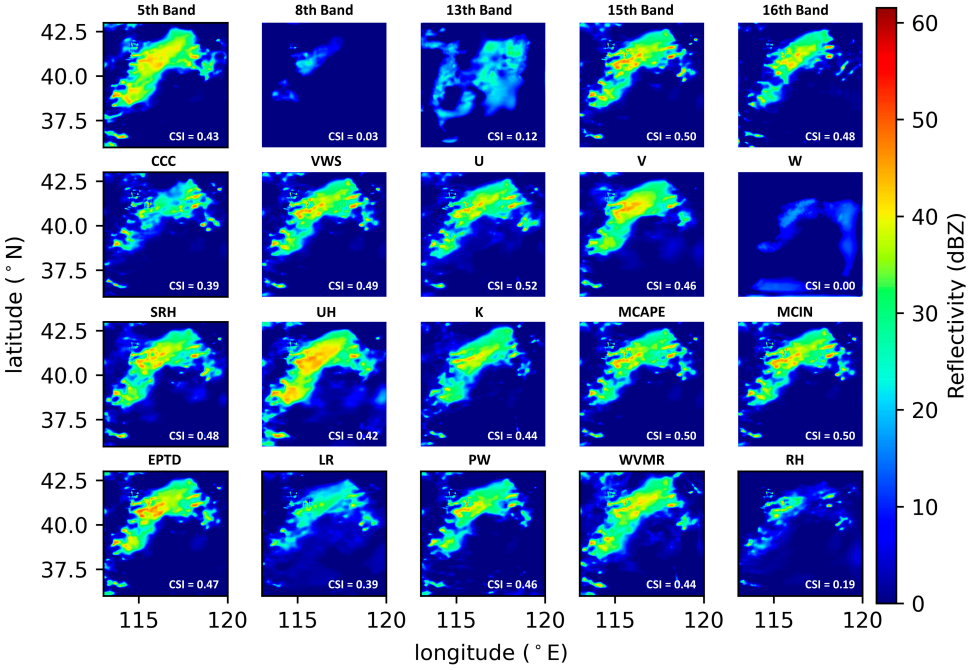

Figure S26. Reconstructions of the radar echo data at 08:30 UTC on 4 September 2016 by the UNet-EW deep network for the SA-b experiments. Each reconstruction is obtained by setting the listed physical quantity to zero while keeping other quantities unchanged.

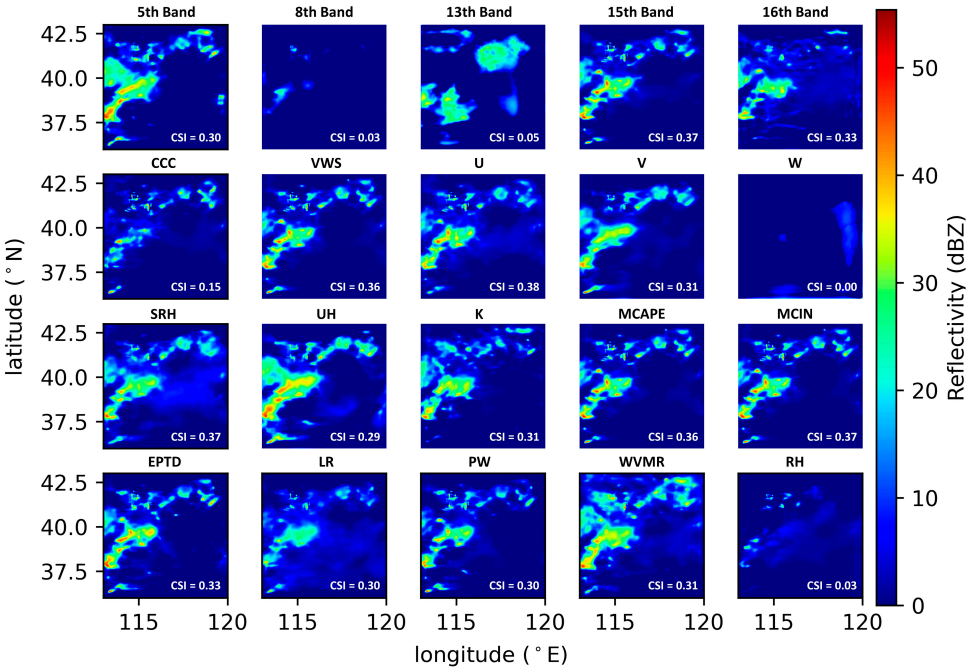

Figure S27. Reconstructions of the radar echo data at 08:00 UTC on 10 September 2016 by the UNet-EW deep network for the SA-b experiments. Each reconstruction is obtained by setting the listed physical quantity to zero while keeping other quantities unchanged.

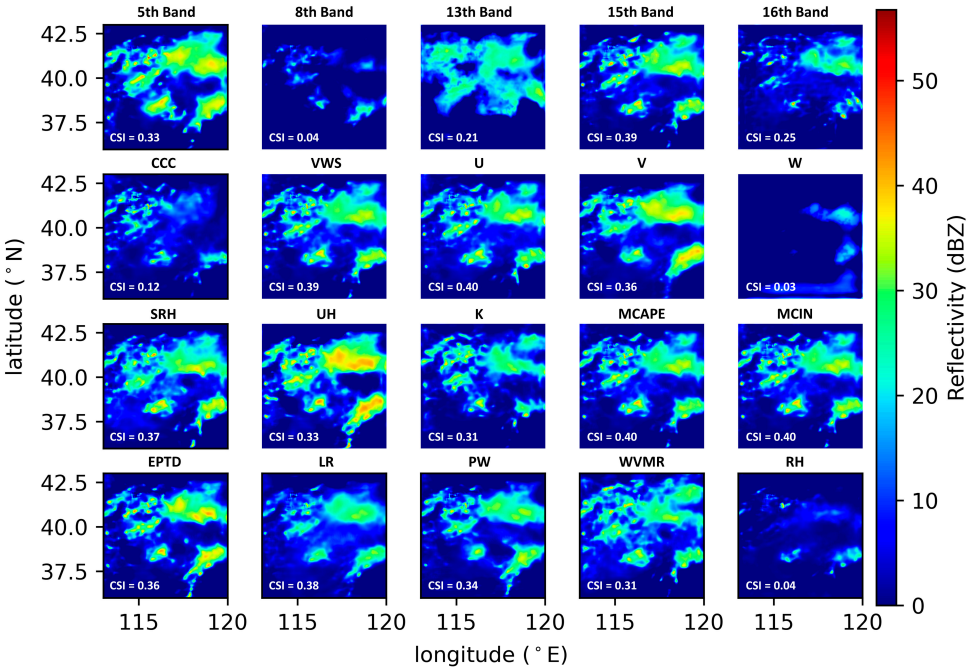

Figure S28. Reconstructions of the radar echo data at 03:30 UTC on 11 September 2016 by the UNet-EW deep network for the SA-b experiments. Each reconstruction is obtained by setting the listed physical quantity to zero while keeping other quantities unchanged.

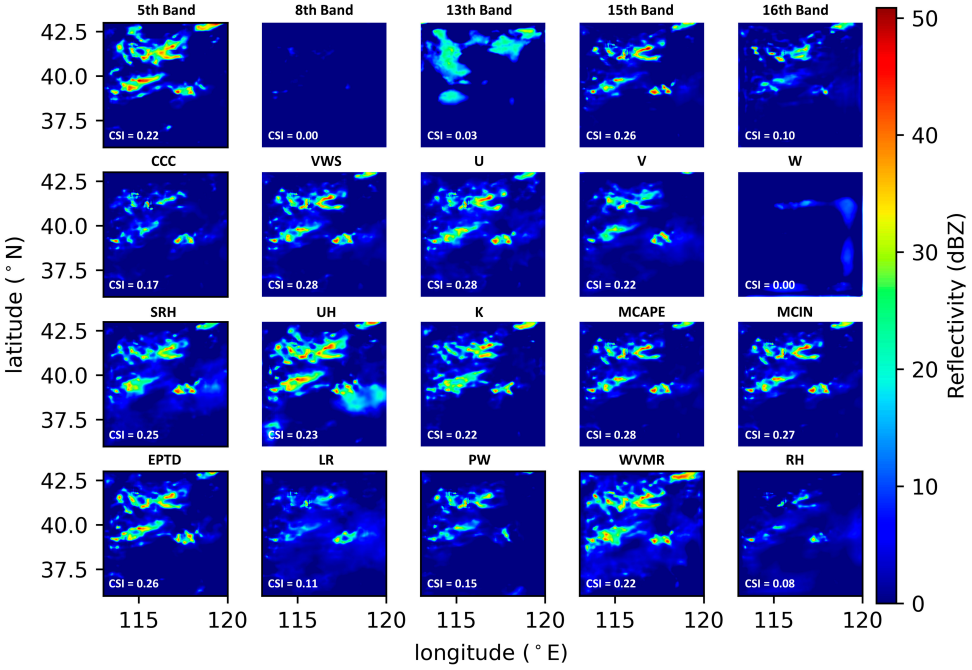

Figure S29. Reconstructions of the radar echo data at 06:30 UTC on 13 September 2016 by the UNet-EW deep network for the SA-b experiments. Each reconstruction is obtained by setting the listed physical quantity to zero while keeping other quantities unchanged.

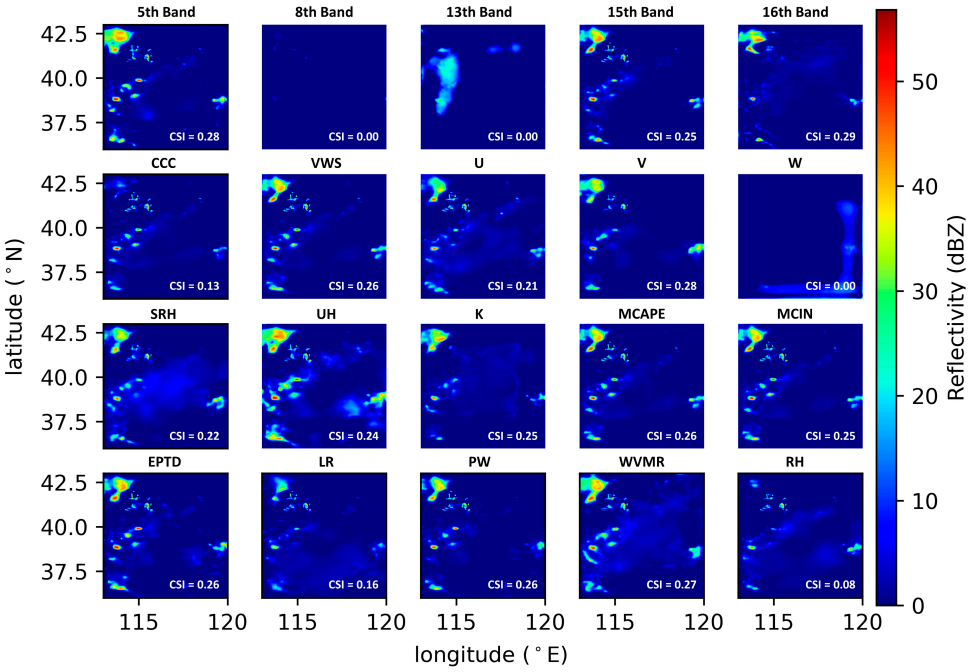

Figure S30. Reconstructions of the radar echo data at 07:30 UTC on 23 September 2016 by the UNet-EW deep network for the SA-b experiments. Each reconstruction is obtained by setting the listed physical quantity to zero while keeping other quantities unchanged.